Molecular Crystals and Liquid Crystals
Publication details, including instructions for authors and subscription information:
http://www.tandfonline.com/loi/gmcl20

Electro-Optic Beam Steering with Nematicons

Raouf Barboza [a] , Alessandro Alberucci [a] & Gaetano Assanto [a]
[a] NooEL, Nonlinear Optics and OptoElectronics Lab, University "Roma Tre", Via della Vasca Navale 84, Rome, Italy
Version of record first published: 18 Apr 2012.

To cite this article: Raouf Barboza , Alessandro Alberucci & Gaetano Assanto (2012): Electro-Optic Beam Steering with Nematicons, Molecular Crystals and Liquid Crystals, 558:1, 12-21

To link to this article: http://dx.doi.org/10.1080/15421406.2011.648069

Mol. Cryst. Liq. Cryst., Vol. 558: pp. 12–21, 2012

ISSN: 1542-1406 print/1563-5287 online
DOI: 10.1080/15421406.2011.648069

Taylor & Francis
Taylor & Francis Group

Electro-Optic Beam Steering with Nematicons

RAOUF BARBOZA,* ALESSANDRO ALBERUCCI, AND GAETANO ASSANTO

NooEL, Nonlinear Optics and OptoElectronics Lab, University "Roma Tre", Via della Vasca Navale 84, Rome- Italy

We analyze a novel geometry expressly designed to maximize the bias-controlled deflection of self-confined light beams in nematic liquid crystals (NLC). We use a self-confined beam and a dielectric interface defined by external voltages, ranging from total internal reflection (TIR) to refraction depending on the applied bias. The optimization of the deflection angle is achieved by using comb electrodes in a planar cell employing planarly oriented NLC molecules. We predict a maximum deflection of 70° with the standard mixture E7.

Keywords Liquid crystals; signal routing; spatial solitons; nematicons; liquid crystal devices

1. Introduction

For their intermediate properties between those of solids and liquids, liquid crystals (LC) are widely used and studied for light manipulation, spanning from the widespread display technology to all-optical signal processing and related applications [1,2]. One of their distinctive properties is the high sensitivity to external disturbances such as electric fields at every frequency, with a high electro-optic response [1] and strong nonlinear optical effects [3]. The main mechanism responsible for their behaviour is molecular reorientation, i.e. the rotation of molecules due to the torque stemming from the interaction between an external electric field and the induced dipole [1,3]. Electro-optics effects have been exploited in the realization of several LC devices for electrically-controlled light-processing, including light sources [4] and passive components such as light valves [5], spatial light modulators [6], tunable photonic crystal fibers [7], tunable lenses [8,9], optical momentum converters [10,11] modulators [12], filters [13], optical controller [14] and so on. In the context of nonlinear optics, their strong interaction with the field combined with the large anisotropy leads to a high nonlinear response, with appreciable effects even for milliwatt input powers [3]; hence, LC represent an ideal workbench for investigating all-optical effects, e.g. nonlinear switching in periodic structures [15] and waveguides [16,17], self-focusing [18]. The latter phenomenon has been extensively studied in the nematic phase, characterized at the molecular level by a significant degree of orientational order, but lacking any long-range positional order [1,3]; when self-focusing counterbalances diffraction-induced spreading, self-confined beams are formed, the latter commonly known as *nematicons* [19–22].

*Address correspondence to Raouf Barboza, NooEL, Nonlinear Optics and Opto-Electronics Lab, Department of Electronic Engineering - University "Roma Tre", Via della Vasca Navale 84, Rome 00146, Italy. E-mail: raouf.barboza@uniroma3.it

Noticeably, relatively low powers (in the mW range) are required to observe light self-trapping and nematicons [19–23]. Due to a diffusive–like process, the strong interaction between NLC molecules yields a light induced perturbation extending well beyond the intensity profiles [3]; thus NLC exhibit a highly nonlocal reorientational response [24], conferring robustness and stability to nematicons, for example avoiding the occurrence of catastrophic collapse [25]. From the applicative point of view, these light-written waveguide can route other weak copolarized signals at different wavelengths [26] or even incoherent in space [27]; the optically-induced guiding channel can be steered by biasing the cell [22,28], with deflection angles equal to the walk-off angle. Moreover, the nematicon path can be modified by introducing localized defects in the dielectric tensor via extra light beams [29] or dielectric interfaces, tunable either electrically [30] or optically [31]. These properties have been used to design and demonstrate reconfigurable interconnections in lightwave circuits [32,33].

In this paper, we detail and numerically analyze a novel scheme for in-plane angular deflection of light-written waveguides in NLC using a graded electrically-tunable interface. With respect to previous configurations [30], this structure allows maximizing the beam deflection taking advantage of in-plane director rotation occurring in the propagation plane of the nematicon [34], achieving an effective angular span of 70° with the aid of comb-patterned electrodes [28,35,36]. The use of nematicons, with typical transverse size of a few microns [20–22,24], permits to increase the effective output resolution (i.e., the number of available spots at the output) with respect to other NLC deflectors in slab waveguides [37].

2. Device Geometry

The proposed geometry is sketched in Fig. 1. An NLC layer of thickness L is confined between two glass slides parallel to the plane yz (Fig. 1(a)). The interfaces between NLC and glass are uniformly rubbed with a suitable polymer for planar anchoring of the molecular director $\hat{n}$ (corresponding to the optic axis [3,20]) at an angle θ_0 with $\hat{z}$ (see inset in Fig. 1(c)).

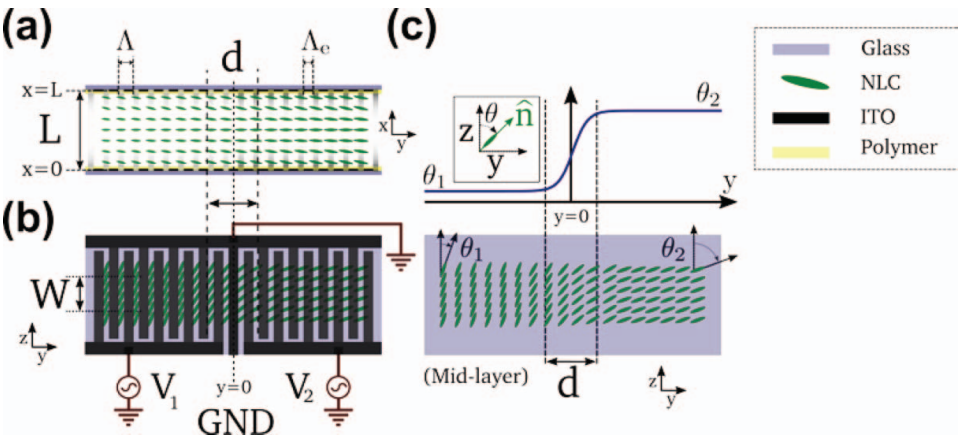

Figure 1. Sketch of the proposed structure. (a) Front view; the superposed gray-scaled map represents the intensity of the low-frequency electric field E_{LF} (darkest colour corresponds to stronger field). (b) Top view. (c) Bottom: distribution of the NLC molecular director in the mid-layer; top: behaviour of θ versus y in $x = L/2$. The inset shows the reference system for the director $\hat{n}$.

On each interface, three comb-shaped electrodes are arranged with fingers parallel to $\hat{z}$: a common ground electrode and two electrodes are biased at V_1 and V_2, respectively, (Fig. 1(b)); the minimum distance between adjacent fingers along y is Λ_e, whereas the period of each comb is 2Λ; hereafter we assume $\Lambda_e/\Lambda = 0.5$. We are interested in the bulk NLC behaviour, neglecting effects connected with input and output interfaces; hence, we will consider the system invariant along z (the results hold valid in the region of length W limited by the two dashed lines in Fig. 1(b)). The electrodes on top and bottom interfaces are aligned along y and, furthermore, it is $\Lambda \ll L$: both these conditions are necessary to minimize the x component of the electric field: when low-frequency biases are applied to the cell, the NLC molecules mainly rotate in the yz plane [3,28,35]. When $V_1 = V_2 = V$ the device behaves essentially as a planar cell with an effective anchoring angle $\theta_0^{eff}(V)$ depending on the applied bias [28,34,35]; when $V_1 \neq V_2$ we expect that orientation θ far away from the interface takes the values $\theta_1 = \theta_0^{eff}(V_1)$ (left side) and $\theta_2 = \theta_0^{eff}(V_2)$ (right side) (see Fig. 2(a)). Therefore, a graded interface will be established along y, with width d fixed by L and a total variation on θ depending on the two applied voltages.

Now we move on to a quantitative estimate of the profile of the electrically-induced interface. Let us name $\theta_{LF}(x, y, V_1, V_2)$ the angular distribution of the director when the only external perturbations are V_1 and V_2 (i.e., in the absence of light); notably, θ_{LF} is sufficient to completely describe the medium properties given the initial assumption of director lying in the plane yz. Making use of the single elastic constant approximation, we obtain the reorientational equation [3,34]:

$$\frac{\partial^2 \theta_{LF}}{\partial x^2} + \frac{\partial^2 \theta_{LF}}{\partial y^2} + \gamma_{LF} \sin(2\theta_{LF}) |E_{LF}|^2 = 0, \tag{1}$$

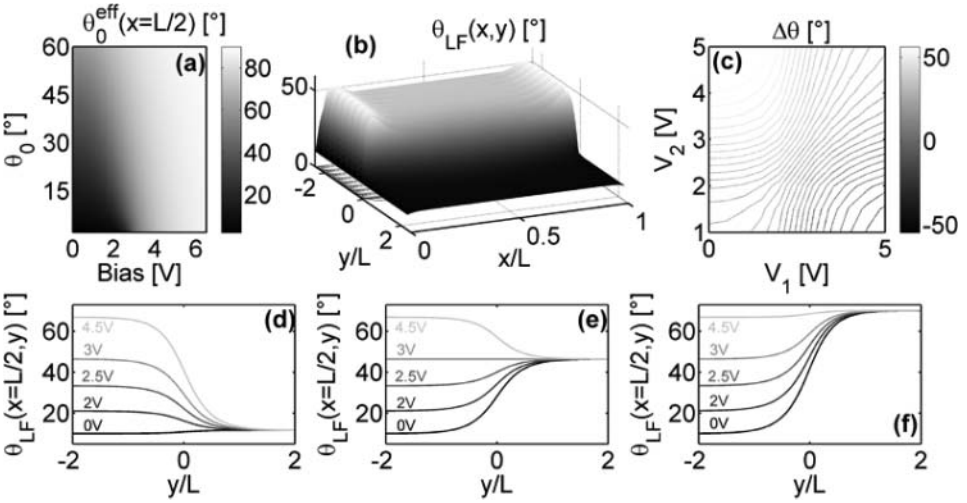

Figure 2. (a) Electro-optic reorientation angle in the cell mid-plane $x = L/2$ when $V_1 = V_2 = V$ versus initial angle θ_0 and applied bias V. (b) θ_{LF} in the xy plane for $V_1 = 3$V and $V_2 = 1$V. (c) Contour plot of $\Delta\theta$ versus V_1 and V_2. (d)–(f) θ_{LF} in the cell mid-plane $x = L/2$ versus y for $V_2 = 1$V (d), $V_2 = 3$V (e) and $V_2 = 5$V (f); the labels indicate V_1 corresponding to each curve. We took $L = 100\,\mu$m and $\sigma = 3.3$.

where E_{LF} is the y-component of the biasing electric field, K is the Frank's equivalent elastic constant [3,20] and $\gamma_{LF} = \Delta\varepsilon_{LF}/(2K)$, with $\Delta\varepsilon_{LF}$ being the low-frequency dielectric anisotropy.

We begin the analysis by noting that, owing to the used excitation scheme (see Fig. 1), the solutions of (1) are symmetric with respect to the cell mid-plane, i.e. $\theta_{LF}|_{x=L/2-a} = \theta_{LF}|_{x=L/2+a}$ $(0 < a < L/2)$; keeping this symmetry in mind, we will limit our considerations to the behavior of θ_{LF} for $0 < x < L/2$. To a first approximation, at the NLC/glass interface (i.e., for $x = 0$) we can take the electric field to be constant and equal to $2V_{1/2}/\Lambda$ between the electrodes, and null beneath them; we also consider an exponential decay along x towards the mid-plane, with a characteristic length l_a, i.e. $\theta_{LF} \propto \exp(-x/l_a)$ [34,35]. Eq. (1) can be conveniently normalized by setting $x' = x/L$, $y' = y/L$, and $V' = \sigma V$, with $\sigma = L/\Lambda$.

The reorientation graphs plotted in Fig. 2(a) versus applied bias show that, for smaller θ_0, a higher bias has to be applied in order to achieve a comparable director distribution; large θ_0 decrease the set of available director positions that can be reached by voltage tuning. Therefore, a trade off between the voltage-sensitivity of reorientational effects (maximum at $\theta_0 = 45^\circ$ [3]) and the maximum achievable discontinuity in the director distribution across the interface has to be found; in the following we take $\theta_0 = 10^\circ$.

We numerically solved Eq. (1) by using a standard Gauss-Seidel relaxation scheme; in the simulations we chose the parameters of the commercial NLC mixture E7, with a corresponding $\gamma_{LF} = 5.4\,\mathrm{V}^{-2}$. With reference to the geometric parameters, we took $L = 100\,\mu$m and $\Lambda = 30\,\mu$m consistently with previous experimental work [28,35], thus providing $\sigma = 3.3$; finally, we considered $l_a/L = 0.05$, the latter value derived from experimental data in this particular geometry [35]. A typical solution for θ_{LF} is plotted in Fig. 2(b): in accordance with Eq. (1), the rotation of $\hat{n}$ occurs everywhere in the same direction (towards the y-axis, see Fig. 1) given that the optical torque depends on $|E_{LF}|^2$. Fast spatial variations of E_{LF} along y at the interface are smoothed out by the nonlocality because $\Lambda \ll L$, providing a flat director distribution around the mid-plane $x = L/2$ along x: in fact, for small variations of θ_{LF} along y and negligible local electric field, Eq. (1) reduces to $d^2\theta_{LF}/dx^2 = 0$, predicting a constant distribution of director $\hat{n}$ along x. As far as the behaviour of θ_{LF} in the proximity of the mid-plane, far from the interface the director along y is uniformly oriented as anticipated, varying monotonically around $y = 0$ on a distance d (see Fig. 1) comparable with L, the latter fixed by the Green's function of the structure [35]; this behaviour is independent on the two applied biases V_1 and V_2, as shown in Fig. 2(d–f). Therefore, the overall jump $\Delta\theta(V_1, V_2) = \theta_2 - \theta_1$ in θ_{LF} as the interface is crossed can be tuned by acting on the two biases V_1 and V_2: the relationship between biases and orientation angles is shown in Fig. 2(c). In essence, the geometry sketched in Fig. 1 allows writing graded dielectric interfaces of width fixed by the cell thickness L and a tunable jump in director orientation, permitting to adjust the refractive index variation and making it either negative or positive, with size as large as the optical anisotropy of the NLC (e.g., 0.2 for E7 and near-infrared excitation).

3. Nematicon Interaction with the Interface

Having established the link between the applied biases and the director distribution in the cell, we can now focus on nonlinear propagation in the mid-plane $x = L/2$. At the input we consider a fundamental Gaussian beam launched in the half-plane $y < -L/2$, i.e., without forces due to the index gradient and acting on it at the entrance; the input wavevector k forms an angle α with $\hat{z}$. The field is polarized along $\hat{y}$ in order to excite only the extraordinary

wave inside the NLC layer [22,34,35]. The latter choice prevents threshold effects in the reorientational response owing to the Fréedericksz transition [3,20,22]. Under these hypotheses, the light twists the molecular director in the plane yz, leading to inhomogeneous changes in the distribution of the optic axis, which feeds back on the beam itself by affecting its width and trajectory. Noteworthy, thanks to its self-confined character, a nematicon remains close to the cell mid-plane, unaffected by diffraction-induced spreading; according to the results previously illustrated in Section 2, the light beam will sense a homogeneous medium along x, with the low-frequency electric field determining only the initial director angle.

Let us set $\theta = \theta_{LF} + \psi$, with ψ the optical contribution to the director reorientation; we also define the magnetic field $\mathbf{H} = A \exp(ik_0 n_0 z)\hat{x}$, with A its slowly varying envelope, k_0 the vacuum wave number and n_0 the refractive index of the carrier [34]. Under the paraxial approximation and in the perturbative nonlinear regime [38], the planar dynamics of the nematicon and the NLC all-optical reorientation in the highly nonlocal regime are described by the 2D model [34,35]:

$$2ik_0 n_0 \left(\frac{\partial A}{\partial z} + \tan\delta \frac{\partial A}{\partial y} \right) + D_y \frac{\partial^2 A}{\partial y^2} + k_0^2 \Delta n_e^2 A = 0 \tag{2}$$

$$\frac{\partial^2 \psi}{\partial z^2} + \frac{\partial^2 \psi}{\partial y^2} - \left(\frac{\pi}{L} \right)^2 \psi + \gamma \sin\left[2(\theta_{LF} + \psi - \delta) \right] |A|^2 = 0 \tag{3}$$

with $\gamma = [\varepsilon_a/(4K)][Z_0/(n_0 \cos\delta)]^2$ (Z_0 is the vacuum impedance and ε_a the optical anisotropy), D_y the diffraction coefficient, δ the walk-off and $n_e(\theta)$ the extraordinary refractive index depending on the local dielectric tensor; $\Delta n_e^2 = n_e^2(\theta) - n_0^2$ is the refractive index change (equivalent to a potential in a particle-like model), including electro-optic (due to θ_{LF}) and all-optical (due to ψ) contributions, the former and the latter responsible for light deflection and self-confinement, respectively [34,35,38].

The nematicon trajectory can be calculated from Eq. (2) via the Ehrenfest's theorem [29,34,35]:

$$\frac{d^2\langle y \rangle}{dz^2} = D_y \frac{n_e}{n_0^2} \left. \frac{\partial n_e}{\partial y} \right|_{\langle y \rangle} + \frac{d \tan\delta}{dz}, \tag{4}$$

where $\langle y \rangle = \int y|A|^2 dy / \int |A|^2 dy$ is the soliton position. Equation (4) rules the transverse motion of the self-confined beams for small tilts of the local wavevector k with respect to $\hat{z}$.

For high deflections Eqs. (2) and (4) hold valid if written in a reference system rotating with the beam, so that the z axis corresponds to the local direction of the wavevector; the last statement implies adiabatic changes in the dielectric tensor [29]. In the highly nonlocal limit and for $\psi \ll \theta_{LF}$ (i.e., a perturbative nonlinear regime [38]) the geometric optics approximation (GOA) can be used to describe the nematicon trajectory [39] independently from input excitation [29,38].

We carried out numerical simulations of the system Eqs. (2 and 3) using an algorithm based upon the Beam Propagation Method (BPM) (for Eq. (2)) and the Gauss-Seidel relaxation scheme (for Eq. (3)). In the computations we considered a piecewise linear profile for the electrically-induced reorientation θ_{LF}, taking $\theta_{LF} = \theta_1$ ($\theta_{LF} = \theta_2$) for $y \le -d/2$ ($y \ge d/2$) and $\theta_{LF} = \theta_1 + (\Delta\theta/d)(y + d/2)$ in the transition region $-d/2 < y < d/2$. From the results discussed in Section 2, we assume $d = L$ and angles θ_{LF} larger than θ_0 and smaller than 90°. A 5 μm-waist Gaussian beam at $\lambda = 1.064$ μm is launched in

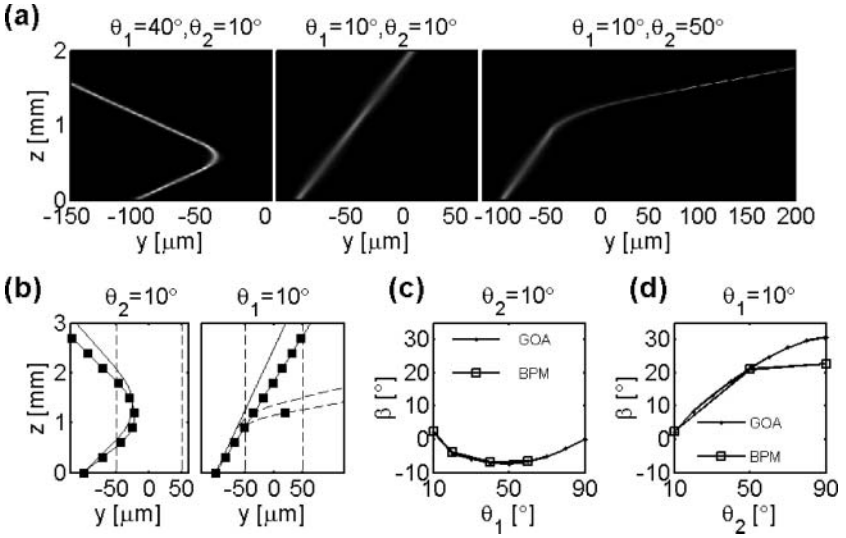

Figure 3. (a) Nematicon evolution in the plane yz for input power P = 3 mW for TIR (left panel), in the absence of interface (mid panel) and in the refracting regime (right panel). (b) Beam trajectories for P = 0.5 mW (solid lines) and P = 3 mW (lines with squares); on the left panel the beam experiences TIR as $\theta_2 = 10^\circ$ and $\theta_1 = 20^\circ$, whereas on the right panel $\theta_1 = 10^\circ$ is kept fixed and light is transmited both for $\theta_2 = 90^\circ$ (dashed lines) and $\theta_2 = 10^\circ$ (solid lines). (c) Soliton output slope β versus θ_1 ($\theta_2 = 10^\circ$) when the nematicon undergoes TIR and (d) β versus θ_2 ($\theta_1 = 10^\circ$) when the nematicon crosses the barrier; here $\alpha = 0^\circ$, P = 0.5 mW and the square (dot) marked lines are BPM (GOA) results.

$y = -100\,\mu$m with k parallel to $\hat{z}$; in this fashion a nematicon, penetrating the graded interface owing to walk-off, propagates over tens of diffraction lengths before interacting with the electrically-written barrier. We stress that the nematicon output angle after its interaction with the inhomogeneity does not depend on the specific shape of the graded interface, in agreement with momentum conservation; the previous statement holds valid for beams much wider than the transition region d [40]. The shape of θ_{LF} determines the lateral displacement of the beam in the output section [34,41].

Figure 3(a) shows the computed nematicon evolution for three values of $\Delta\theta$, corresponding to reflection, absence of barrier and refraction. In all cases, the changes in the dielectric tensor are slow enough to guarantee the nematicon survival within the barrier, with negligible power losses. Independently from $\Delta\theta$, at the beginning the solitons propagate towards the interface due to the walk-off, experiencing a zero index gradient. When light hits the interface in $y = -d/2$, the forces due to longitudinal changes in walk-off and the transverse index gradient begin to act on the soliton, as described by Eq. (4): for $\theta_1 > \theta_2$ the index gradient is negative and at the interface the wavevector bends towards $y < 0$; for $\theta_1 = \theta_2$ the light trajectory is straight as the medium is homogeneous; finally, for $\theta_1 < \theta_2$ the solitons always overcome the barrier, with the index gradient pushing them towards $y > 0$. The simulations show that the dominant contribution in soliton deflection is played by refractive index gradient, when compared with longitudinal changes in walk-off. To achieve TIR in the case $\theta_1 > \theta_2$, the change in transverse k has to be large enough to ensure an output Poynting vector S with a negative component along $\hat{y}$. Noteworthy, in TIR reflection and incidence angles are generally different owing to anisotropy [42]. Figure 3(b)

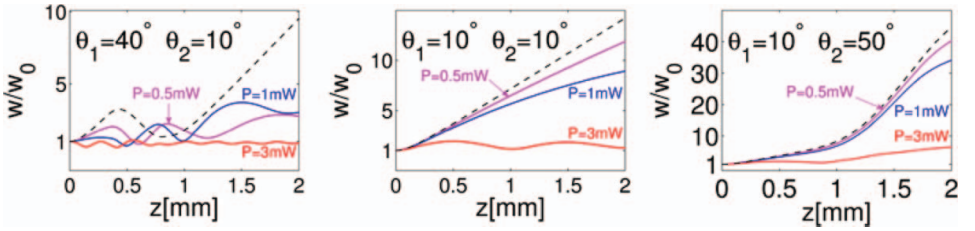

Figure 4. Beam width w normalized with respect to the input waist $w_0 = 5\,\mu$m for various input powers and angles θ_1 and θ_2 corresponding to the plots in Fig. 3 (see labels: dashed lines = linear propagation).

graphs calculated nematicon trajectories versus power: the power dependence is mainly due to nonlinear changes in walk-off [38,41].

Let us define β as the output angle (that is, when the interaction with the interface is ceased) of the Poynting vector with respect to $\hat{z}$; Fig. 3(c) [Fig. 3(d)] plots the output angles β for a reflecting [refracting] interface versus θ_1 [θ_2] for an assigned $\theta_2[\theta_1]$, the latter equal to $\theta_0 = 10^\circ$ to maximize deflection. Figure 3(c and d) compares BPM and GOA predictions, showing a very good agreement between the two approaches up to $\beta = 20^\circ$, when BPM fails due to non-paraxial effects [29,34].

For applications we are interested in the overall steering available for a given structure, i.e., for a fixed θ_0, when the applied biases are changed; clearly, such angle will be the sum of the absolute maximum of β calculated from Fig. 3(c) and the one from Fig. 3(d): the total available steering is about 40° for initial wavevector parallel to the interface. Finally, Fig. 4 shows the nematicon waist versus z, demonstrating how the size of the optically-induced waveguide can be easily controlled via the input power [35].

It is natural to investigate the performances when nematicons impinge with a tilted wavevector on the graded interface. Let α be the angle of the input wavevector with axis z; we limit our considerations to $\alpha > 0$, i.e., nematicons propagating towards the graded interface. We are mainly interested on the trajectory; hence, we use only GOA, as non-paraxial BPM codes require large computational efforts [43]. Moreover, since we already demonstrated with BPM in the case $\alpha = 0$ that nematicons survive the interaction with the interface without appreciable losses, we extend this to the case $\alpha \neq 0$; experiments carried out at non-planar interfaces support this approximation [30,41,42].

Results from GOA are plotted in Fig. 5. To achieve wide-angle steering α has to be chosen in order to ensure nematicon TIR for at least one pair of angles $\theta_{1/2}$, i.e., of applied biases $V_{1/2}$. In fact, for angles α spanning from grazing ($\alpha = 0^\circ$) to normal incidence ($\alpha = 90^\circ$) there will be a threshold incidence angle $\alpha_{TIR}^{\max}$: beyond this TIR is forbidden for every director orientation. Figure 5(a) shows α_{TIR}, defined as the maximum angle α ensuring TIR for assigned θ_1 and θ_2: each curve defines the existence domain for TIR, with points below (above) the curves corresponding to the presence (absence) of TIR. For $\theta_1 \to 0^\circ$ TIR takes place only in the proximity of $\alpha = 0^\circ$ and for $\theta_2 < \theta_1$ (actually, for $\theta_1 = 0^\circ$ a collimated beam does not interact with the interface), whereas for increasing θ_1 the incidence angle allowing TIR increases as well, reaching the maximum for $\theta_1 = 90^\circ$. This agrees with the refractive index dependence on director orientation, the index being maximum for θ_1 close to 90°; noteworthy, α_{TIR} decreases with θ_2 for the same reason. From Fig. 5(a), $\alpha_{TIR}^{\max}$ occurs for $\theta_1 = 90^\circ$ and $\theta_2 = 0^\circ$, with a value of 25.1° for E7 in the near-infrared.

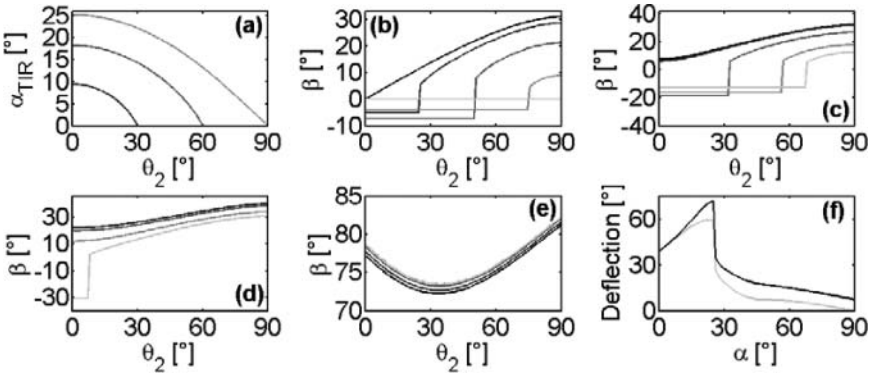

Figure 5. (a) α_{TIR} versus θ_2 for $\theta_1 = 0°, 30°, 60°$ and $90°$, lines from dark to bright, respectively. Output angle β versus θ_2 for: (b) $\alpha = 0°$, (c) $10°$, (d) $25°$ and (e) $80°$; lines correspond to $\theta_1 = 0°, 25°, 50°, 75°$ and $90°$ from dark to bright, respectively. (f) Maximum angular deflection of wavevector $\boldsymbol{k}$ (gray line) and Poynting vector $\boldsymbol{S}$ (black line) versus α for θ_1 and θ_2 ranging from $0°$ to $90°$.

Figures 5(b–e) display output angles β for a fixed α. For $\alpha = 0°$ (see Fig. 5(b)) the nematicon undergoes TIR for $\theta_1 > 0°$, whereas for larger θ_1 TIR occurs when $\theta_2 < \theta_1$, corresponding to an index gradient repelling the beam; in the β curves the occurrence of TIR causes a discontinuity, with β depending only on θ_1 (i.e., the refractive index in the incidence medium) when TIR takes place. Conversely, in the refractive regime β increases with θ_2 due to a larger index gradient pushing the nematicon to the right. For $\alpha = 10°, 25°$ (Fig. 5(c and d)) TIR occurs in a smaller set of $\theta_{1/2}$, consistently with Fig. 5(a) and retaining the qualitative behaviour of the case $\alpha = 0°$, β constant in the TIR regime and growing when the nematicon is refracted. Quantitatively, β in TIR is approximately equal to $-\alpha$ (neglecting non-specular reflection due to anisotropy and contributions due to walk-off [42]), much larger than for $\alpha = 0°$. Finally, for $\alpha = 80°$ (Fig. 5(e)) the overall steering angle is much lower than in previous cases owing to the absence of TIR, in agreement with Fig. 5(a). Noteworthy, the behaviour of β versus θ_2 is no longer monotonic due to walk-off contributions on the nematicon Poynting vector.

Figure 5(f) summarizes the maximum angular deviation for an assigned incidence angle α: the maximum occurs for $\alpha = \alpha_{TIR}^{\max}$ and the available span is about $70°$, much larger than the $40°$ reported with non-planar deflection [42]. After the peak, the available maximum deflection reduces abruptly due to the lack of TIR.

4. Conclusions

We have analyzed a new scheme for electro-optic light steering in NLC based on planar deflection of nematicons, corresponding to light written waveguides. A graded index interface defined in NLC with comb interdigitated electrodes allows controlling both the size and the sign of the induced barrier. The high electro-optic response of NLC permits to tune the dielectric properties of the medium with low-voltages.

Co-planarity between nematicons and bias-controlled molecular reorientation allows maximizing the angular span for a given material, at variance with previous geometries where the interaction was three-dimensional. Overall steering angles as large as $70°$ can be reached in E7 by using refraction and TIR. Finally, self-focusing and light self-trapping can

optimize signal confinement and the number of spots distinguishable at the exit, enhancing the spatial resolution of the proposed configuration.

References

[1] Yang, D. K., & Wu, S. T. (2006). *Fundamentals of Liquid Crystal Devices*, Wiley: New York.
[2] Woltman, S. J., Jay, J. D., & Crawford, G. P. (2007). Liquid crystals: frontiers in biomedical applications. World Scientific: Singapore.
[3] Khoo, I. C. (2009). *Phys. Rep.*, *471*, 221–267.
[4] Coles, H., & Morris, S. (2010). *Nat. Photonics*, *4*, 676–685.
[5] Margerum, J. D., Nimoy, J., & Wong, S.-Y. (1970). *Appl. Phys. Lett.*, *17*, 51–53.
[6] Liu, H.-K., Davis, J. A., & Lilly, R. A. (1985). *Opt. Lett.*, *10*, 635–637.
[7] Du, F., Lu, Y.-Q., & Wu, S.-T. (2004). *Appl. Phys. Lett.*, *85*, 2181–2183.
[8] Sato, S. (1999). *Opt. Rev.*, *6*, 471–485.
[9] Valley, P., Mathine, D. L., Dodge, M. R., Schwiegerling, J., Peyman, G., & Peyghambarian, J. (2010). *Opt. Lett.*, *35*, 336–338.
[10] Marrucci, L. (2008). *Mol. Cryst. Liq. Cryst.*, *488*, 148–162.
[11] Brasselet, E., & Loussert, C. (2011). *Opt. Lett.*, *36*, 719–721.
[12] Cotter, L. K., Drabik, T. J., Dillon, R. J., & Handschy, M. A. (1990). *Opt. Lett.*, *15*, 291–293.
[13] Gilardi, G., Asquini, R., D'Alessandro, A., & Assanto, G. (2010). *Opt. Express*, *18*, 11524–11529.
[14] Tabiryan, N. V., Nersisyan, S. R., White, T. J., Bunning, T. J., Steeves, D. M., & Kimball, B. R. (2011). *AIP Advances*, *1*, 022153.
[15] Laudyn, U. A., Miroshnichenko, A. E., Krolikowski, W., Chen, D. F., Kivshar, Y. S., & Karpierz, M. A. (2008). *Appl. Phys. Lett.*, *92*, 203304.
[16] Fratalocchi, A., & Assanto, G. (2005). *Appl. Phys. Lett.*, *86*, 051109.
[17] D'Alessandro, A., Asquini, R., Trotta, M., Beccherelli, R., & Khoo, I. C. (2010). *Appl. Phys. Lett.*, *97*, 093302.
[18] Braun, E., Faucheux, L. P., & Libchaber, A. (1993). *Phys. Rev. A*, *48*, 611–622.
[19] Peccianti, M., De Rossi, A., Assanto, G., De Luca, A., Umeton, C., & Khoo, I. C. (2000). *Appl. Phys. Lett.*, *77*, 7–9.
[20] Assanto, G., & Peccianti, M. (2003). *IEEE J. Quantum Electron.*, *19*, 13–21.
[21] Assanto, G., & Karpierz, M. A. (2009). *Liq. Cryst.*, *36*, 1161–1172.
[22] Peccianti, M., Conti, C., Assanto, G., De Luca, A., & Umeton, C. (2004). *Nature*, *432*, 733–737.
[23] Warenghem, M., Blach, J. F., & Henninot, J. F. (2008). *J. Opt. Soc. Am. B.*, *25*, 1882–1887.
[24] Conti, C., Peccianti, M., & Assanto, G. (2003). *Phys. Rev. Lett.*, *91*, 073901.
[25] Kivshar, Y. R., & Agrawal, G. P. (2003). *Optical Solitons*, Academic Press: San Diego.
[26] Peccianti, M., & Assanto, G. (2001). *Opt. Lett.*, *26*, 1690–1692.
[27] Peccianti, M., & Assanto, G. (2001). *Opt. Lett.*, *26*, 1791–1793.
[28] Piccardi, A., Peccianti, M., Assanto, G., Dyadyusha, A., & Kaczmarek, M. (2009*). Appl. Phys. Lett.*, *94*, 091106.
[29] Alberucci, A., Piccardi, A., Bortolozzo, U., Residori, S., & Assanto, G. (2010). *Opt. Lett.*, *35*, 390–392.
[30] Peccianti, M., Dyadyusha, A., Kaczmarek, M., & Assanto, G. (2006). *Nature Phys.*, *2*, 737–742.
[31] Piccardi, A., Assanto, G., Lucchetti, L., & Simoni, F. (2008). *Appl. Phys. Lett.*, *93*, 171104.
[32] Piccardi, A., Alberucci, A., Bortolozzo, U., Residori, S., & Assanto, G. (2010). *IEEE Photon. Techn. Lett.*, *22*, 694–696.
[33] Piccardi, A., Alberucci, A., Bortolozzo, U., Residori, S., & Assanto, G. (2010). *Appl. Phys. Lett.*, *96*, 071104.
[34] Barboza, R., Alberucci, A., & Assanto, G. (2011). *Opt. Lett.*, *36*, 2725–2727.
[35] Alberucci, A., Piccardi, A., Peccianti, M., Kaczmarek, M., & Assanto, G. (2010). *Phys. Rev. A*, *82*, 023806.
[36] Soref, R. A. (1974). *J. Appl. Phys.*, *45*, 5466–5468.

[37] Davis, S. R., Farca, G., Rommel, S. D., Martin, A. W., & Anderson, M. (2008). *Proc. SPIE*, *6971*, 69710G.
[38] Piccardi, A., Alberucci, A., & Assanto, G. (2011). Nematicons self-steering. *Mol. Cryst. Liq. Cryst.*, in press.
[39] Sluijter, M., De Boer, D. K. G., Urbach, H. P., Strömer, J. & Cennini, G. (2009). *Proc. SPIE*, *7232*, 72320S.
[40] Depine, R. A., & Bonomo, N. E. (1995). *J. Mod. Opt.*, *42*, 2401–2412.
[41] Peccianti, M., Assanto, G., Dyadyusha, A., & Kaczmarek, M. (2007). *Opt. Lett.*, *32*, 271–273.
[42] Peccianti, M., Assanto, G., Dyadyusha, A., & Kaczmarek, M. (2007). *Phys. Rev. Lett.*, *98*, 113902.
[43] Sánchez-Curto, J., Chamorro-Posada, P., & McDonald, G. S. (2007). *Opt. Lett.*, *32*, 1126–1128.